ELSEVIER

Journal of Fluids and Structures 24 (2008) 700–719

JOURNAL OF FLUIDS AND STRUCTURES

www.elsevier.com/locate/jfs

Self-sustained aeroelastic oscillations of a NACA0012 airfoil at low-to-moderate Reynolds numbers ☆

D. Poirel*, Y. Harris, A. Benaissa

Department of Mechanical Engineering, Royal Military College of Canada, PO Box 17000, Station Forces, Kingston, Ont. Canada K7K 7B4

Received 14 September 2006; accepted 22 November 2007
Available online 4 March 2008

Abstract

A wind tunnel experimental investigation of self-sustained oscillations of an aeroelastic NACA0012 airfoil occurring in the transitional Re regime is presented. To the authors' knowledge this is the first time that aeroelastic limit cycle oscillations (LCOs) associated with low Re effects have been systematically studied and reported in the public literature. While the aeroelastic apparatus is capable of two-degree-of-freedom pitch-plunge motion, the present work concerns only the motion of the airfoil when it is constrained to rotate in pure pitch. The structural stiffness is varied as well as the position of the elastic axis; other parameters such as surface roughness, turbulence intensity and initial conditions are also briefly discussed. In conjunction with the pitch measurements, the flow is also recorded using hot-wire anemometry located in the wake at a distance of one chord aft of the trailing edge. It is observed that for a limited range of chord-based Reynolds numbers, $4.5\times10^4\leqslant \mathrm{Re}_c\leqslant 1.3\times10^5$, steady state self-sustained oscillations are observed. Below and above that range, these oscillations do not appear. They are characterized by a well-behaved harmonic motion, whose frequency can be related to the aeroelastic natural frequency, low amplitude ($\theta_{\max}<5.5^\circ$) and some sensitivity to flow perturbations and initial conditions. Furthermore, hot-wire measurements for the wing held fixed show that no periodicity in the undisturbed free-stream nor in the wake account for the oscillations. Overall, these observations suggest that laminar separation plays a role in the oscillations, either in the form of trailing edge separation or due to the presence of a laminar separation bubble.

Keywords: Self-sustained oscillations; Aeroelasticity; LCO; Low Re aerodynamics; NACA0012

1. Introduction

Whereas the majority of reported experimental investigations on self-sustained oscillations of either pitch-plunge or pitch-flap aeroelastic wings in subsonic flow have targeted the effect of structural nonlinearities in a first instance (Marsden and Price, 2005; O'Neil et al., 1996) and as a secondary matter dynamic stall or stall flutter at high angle of attack (Tang and Dowell, 1992; Dowell et al., 2003), few have focused on the impact of nonlinear aerodynamic

☆ An earlier version of this paper was presented in the 7th FSI, AE and FIV + N Symposium, held within the 2006 PVP Conference in Vancouver, BC, Canada.

*Corresponding author. Tel.: +1 613 541 6000x6452.
E-mail address: poirel-d@rmc.ca (D. Poirel).

0889-9746/$ - see front matter © 2008 Elsevier Ltd. All rights reserved.
doi:10.1016/j.jfluidstructs.2007.11.005

Nomenclature

a_h	nondimensional distance (by half chord, b) between mid-chord and elastic axis, positive going aft
AR	aspect ratio, s/c
b	half chord (m)
c	airfoil chord length (m)
C_{Mea}	aerodynamic moment coefficient about the elastic axis
D_s	viscous structural damping coefficient (N m s)
e	distance between the aerodynamic centre (AC) and elastic axis (EA); positive going aft (m)
f	frequency (Hz)
I_s	mass moment of inertia of rotating parts about elastic axis (kg m^2)
k	reduced frequency, $k=\omega b/U$
K_a	aerodynamic stiffness coefficient (N m)
K_T	total stiffness coefficient (N m)
K_s	structural stiffness coefficient (N m)
L	lift (N)
m_θ	mass of parts in rotation (kg)
$M_{\mathrm{C/4}}$	aerodynamic moment about the quarter-chord (N m)
M_{EA}	aerodynamic moment about the elastic axis (N m)
Re_c	Reynolds number based on airfoil chord
s	wing span (m)
St_T	Strouhal number based on airfoil thickness, fT/U (cycle)
T	airfoil thickness (m)
Tu	turbulence intensity, u'_{rms}/U
U	free-stream airspeed (m/s)
u'	unsteady longitudinal flow velocity (m/s)
v'	unsteady vertical flow velocity (m/s)
x_θ	nondimensional distance (by half chord, b) between elastic axis and centre of mass of rotating parts, positive going aft
α	angle of attack (deg)
β	real part of eigenvalue, $-\zeta\omega_n$ (rad/s)
ζ_s	structural damping ratio, $D_s/(2I_s\omega_\theta)$
θ	pitch angle (deg or rad)
μ	airfoil/air mass ratio, $m_\theta/(\pi\rho s b^2)$
Φ_{uu}	unsteady longitudinal flow velocity PSD
Φ_{vv}	unsteady vertical flow velocity PSD
$\Phi_{\theta\theta}$	pitch response PSD
ω	radial frequency (rad/s)
ω_n	undamped aeroelastic natural frequency (rad/s)
ω_θ	undamped structural natural frequency, $\sqrt{K_s/I_s}$ (rad/s)

phenomena, occurring at low-to-moderate Reynolds numbers, on the aeroelastic behaviour. In this range of Reynolds numbers, $10^4 \leqslant \mathrm{Re}_c \leqslant 10^6$, complex viscous phenomena occur such as laminar boundary layer separation leading to the formation of a laminar separation bubble (LSB), transition of the laminar shear layer, and subsequent reattachment of the turbulent layer (Gad-el-Hak, 1990; Mueller, 1985). The richness and complexity of low-to-moderate Reynolds number flows have the potential to significantly impact the aeroelastic dynamics, perhaps in some ways analogous to the extensively studied, but yet to be fully solved, transonic regime problem encountered on fighter aircraft. The interest in this regime of Reynolds number is therefore two-fold. It is of a fundamental nature due to the complexity of the viscous phenomena involved. It is also of a practical nature since a wide range of unmanned air vehicles (UAVs) operate in these flow conditions. This is so due to their small size or low-density atmosphere. Moreover, many UAV platforms are very flexible, making them prone to aeroelastic deformations. In the following paragraphs, a focussed review on some relevant aerodynamic characteristics of airfoils at low-to-moderate Reynolds numbers is presented. It is complemented by a historical summary of reported aeroelastic oscillations of wings whose origin appears to be linked to low-to-moderate Re aerodynamics. In this work, the terms low-to-moderate Re flow and transitional flow are used interchangeably, whereby transition is understood in the general sense; it is not limited to boundary layer transition but includes free-shear layer transition [or separated-flow transition (White, 2006)] and wake vortex-shedding transition.

1.1. Stall types and general characteristics

The existence of a LSB is generally associated with the so-called *thin-airfoil stall*; stall being defined at the angle of attack for maximum lift. Thin-airfoil stall is one of the three basic types of (static) stall according to the classification of McCullough and Gault (1951). It is defined as such: ''thin-airfoil stall is preceded by a laminar separation near the leading edge, with turbulent reattachment at a point which moves progressively rearward with increasing incidence''. Further increase in angle of attack results in the flow being completely detached. The sequence of events occurs gradually, resulting in a continuous and slowly decreasing post-stall lift coefficient (C_L). At higher Reynolds numbers the presence of a LSB is less likely (although it has been shown to exist for very thin airfoils with a small nose radius such as the NACA64A0006 at $\mathrm{Re}_c = 5.8\times10^6$ (Tani, 1964); in fact, all tests performed by McCullough and Gault were

done at this single Reynolds number). Depending on its geometry, amongst other factors, an airfoil may then experience *trailing-edge stall* or *leading-edge stall*, which are the two other basic stall types according to McCullough and Gault. Trailing-edge stall is "preceded by a movement of the separation point of the turbulent boundary layer forward from the trailing edge with increasing incidence". In this case, transition of the boundary layer, which is advanced due to the higher Reynolds numbers, occurs ahead of the theoretical laminar boundary layer separation point, had laminar separation occurred otherwise. The turbulent boundary layer having more momentum is able to penetrate deeper into the adverse pressure gradient region. The stall angle is increased and the lift curve is also continuous. On the other hand, leading-edge stall is "caused by an abrupt separation of the laminar boundary layer near the leading edge without subsequent reattachment", or by a short LSB close to the leading edge which bursts at stall (as opposed to a long bubble for thin-airfoil stall) (Gad-el-Hak, 1990; Tani, 1964). Hence, contrary to the two previous cases, the lift coefficient decreases sharply, even discontinuously, at stall and is often associated with a hysteric relationship between C_L and α (Gad-el-Hak, 1990). We add that McCullough and Gault's classification system builds on the earlier pioneering definitions of Jones (1933), who was, however, experimentally limited in his ability to relate stall type to boundary layer state. Furthermore, the actual stall characteristics exhibited by a particular airfoil for certain conditions may not fit exactly any of the three basic types; a combination of stall types may exist.

A simple examination of the C_L versus α curves obtained by Jacobs and Sherman (1937) in a variable density tunnel tends to indicate that the NACA0012 stall characteristics change from thin-airfoil stall to leading-edge stall at about a critical $\mathrm{Re}\sim 1\times 10^6$. More recent and detailed experimental results from Huang and Lee (1999) shed additional light on the sub-million Re regime for the NACA0012 airfoil. For a turbulence intensity of 0.2% and $\mathrm{Re}_c = 5.9\times 10^4$, surface-oil flow patterns reveals the presence of a LSB for angles of attack just larger than 2° and moving forward with increasing angle of attack, as well as turbulent trailing edge separation with the separation point also moving forward with increasing incidence. In addition, the rate of advancement with angle of attack of the reattachment point is larger than for the separation point, resulting in the length of the LSB decreasing with angle of attack. This behaviour is also observed for two higher Reynolds numbers, $\mathrm{Re}_c = 9.5\times 10^4$ and 1.4×10^5. The combined presence at stall of a small bubble near the leading edge and a turbulent trailing edge separation suggests that the stall characteristics at these Reynolds numbers is a combination trailing-edge/leading-edge stall type, rather than thin-airfoil stall.

This combination of stall types has been reported by Broeren and Bragg (2001) for a Clark-Y airfoil, which also has a 12% thickness but a 3.55% camber. Broeren and Bragg investigated experimentally the unsteady characteristics of thin airfoils near (static) stall. Tests were carried out at $\mathrm{Re}_c = 3\times 10^5$ and $\mathrm{Tu} = 0.1\%$. They noted a correlation between the existence of a LSB, found for thin-airfoil stall and combination thin-airfoil/trailing-edge stall, and large fluctuations of the lift coefficient. For thin-airfoil stall the lift fluctuation intensity, defined here as $C'_{L\mathrm{rms}}/C_{L\max}$ where $C'_{L\mathrm{rms}}$ is the r.m.s. of the lift coefficient unsteady fluctuations, is about 6%; for instance it is $0.06/0.92 = 6.5\%$ for the NACA0009 airfoil. For the combination thin-airfoil/trailing-edge stall the lift fluctuation intensity hovers around 12%. Broeren and Bragg speculated that the trailing edge separation, in the case of this combination type stall, amplifies the unsteady effects otherwise caused by the LSB. In the three other cases identified in their experiment, namely trailing-edge stall, leading-edge stall and combination trailing-edge/leading-edge, where a long LSB is not involved, the fluctuations were much less severe, an order of magnitude lower. For instance the Clark-Y airfoil, which exhibited a combination trailing-edge/leading-edge stall type, had a lift fluctuation intensity of 0.4%.

In addition to these large broadband fluctuations in lift, Broeren and Bragg observed a clear periodicity in the lift spectrum, whose main characteristic was an unusually low frequency. The first reported indication of such oscillations appears to be that of Jones (1933). However, it is only some 50 years later that a systematic study was undertaken. Zaman et al. (1989) observed low frequency oscillations of the flow on the upper surface of a rigidly mounted LRN-1007 wing at angles of attack near stall, and which corresponded to a Strouhal number $\mathrm{St}\approx 0.02$. Tests were conducted at $1.5\times 10^4 \leqslant \mathrm{Re}_c \leqslant 3.0\times 10^5$ and for different wing profiles. Note that the LRN-1007 profile was later classified by Broeren and Bragg (2001) as exhibiting combination thin-airfoil/trailing-edge stall. They remarked that the occurrence of these oscillations had been "illusive" and "puzzling"; the oscillations were very sensitive to ambient conditions such as free-stream turbulence, to acoustic excitation and to boundary layer tripping. Zaman et al. were also able to trigger these flow oscillations on a NACA0012 wing but only after considerable trial using boundary layer tripping on the pressure side. They also noted that the oscillation amplitude was large, especially in the vicinity of the wing quarter chord point and decreased steadily downstream. They argued that the origin of these low frequency oscillations was a transitional state of the boundary layer, between laminar and fully turbulent, which then affected the susceptibility of the wing to flow separation. They further argued that the phenomenon was likely related to stall flutter as it involves periodic stalling and unstalling. Bragg et al. (1993, 1995) continued the investigation into the low frequency flow oscillation and suggested that the phenomenon was related to a cyclic growth and bursting of the LSB. They also obtained results showing that the flowfield during the unstalled part of the cycle was two-dimensional. Subsequent studies by Broeren and Bragg (1998, 2001) confirmed the fundamental role of the LSB. In addition to the important lift

fluctuation intensity discussed previously, they reported Strouhal numbers as low as 0.007 for a NACA0009. Power spectral analysis of the flow measured in the wake at about one chord aft of the trailing edge showed little energy at these low frequencies and thus confirmed that the origin of the oscillations was not in the wake.

1.2. Pre-stall behaviour

Lutz et al. (2001) also noted chordwise temporal oscillations of the LSB but for small pre-stall angles, $\alpha \approx 4$–5°. Tests were performed on a NACA0009 at $Re_c = 5 \times 10^4$ and $Tu < 0.08\%$. They labelled these oscillations as flapping since a clear periodicity could not be distinguished. They did not pursue this further. Of additional interest in their work is the significantly nonlinear C_L versus α relationship even well below the stall angle. This is shown in Fig. 1. Also shown for comparison are the inviscid thin-airfoil theory lift curve, whose slope is 2π, as well as the theoretical curve accounting for airfoil thickness (Abbott and von Doenhoff, 1959). Accounting for the airfoil thickness has for effect to increase slightly the inviscid lift coefficient. However, considering the presence of a boundary layer at high Reynolds numbers, the nonviscous flow would be distorted even though no LSB, nor low angle of attack trailing edge separation, would be expected. In this case, the overall effect would still be a reasonably linear lift curve, but with a smaller slope thus cancelling any gain due to the airfoil thickness. As depicted in Fig. 1, the low Reynolds number behaviour is more complex.

The next figure is also adapted in part from Lutz et al. (2001). Shown are the measured pressure distributions on the suction side of the airfoil. We have added the nonviscous solution calculated using the simple engineering method proposed by Abbott and von Doenhoff (1959). The inviscid solution helps in gaining a physical insight into the viscous effects.

For very low angles of attack ($\alpha < 3^\circ$), the lift curve slope is about half the theoretical value. This is attributed to trailing edge separation and confirmed by a constant pressure coefficient distribution, C_p, at the trailing edge on the suction side. For angles above 3° a LSB appears, also indicated by a plateau on the suction side C_p distribution and which moves upstream with angle of attack. For instance, the position of the bubble is indicated in Fig. 2 for $\alpha = 4^\circ$. The symbol "S" refers to the laminar separation point; transition of the shear layer is shown by "T"; reattachment of the turbulent boundary layer occurs at "R". Concurrently to the appearance of the LSB, the lift curve slope increases to its inviscid value. It decreases again for $\alpha > 5^\circ$ until stall occurs at $\alpha = 9^\circ$. The loss of lift is continuous and moderate. For angles of attack close to stall, the LSB occurs near the leading edge right after the point of minimum pressure since the laminar boundary layer cannot sustain a large adverse pressure gradient. Lutz et al. mention the presence of turbulent trailing edge separation near stall. It is, however, difficult to ascertain their claim based on the C_p distributions presented. The pre-stall behaviour of the surface flow around the airfoil possesses some characteristics of thin-airfoil stall and combination thin-airfoil/trailing-edge stall, as well as trailing-edge/leading-edge stall. It is not possible to provide a more definite picture of the stall type since the largest angle of attack for which the pressure distribution is given is 8°. Of certainty, however, are the nonlinear behaviour of the lift curve at pre-stall angles of attack, as well as the related trailing edge laminar separation and the subsequent laminar separation bubble. This behaviour was also

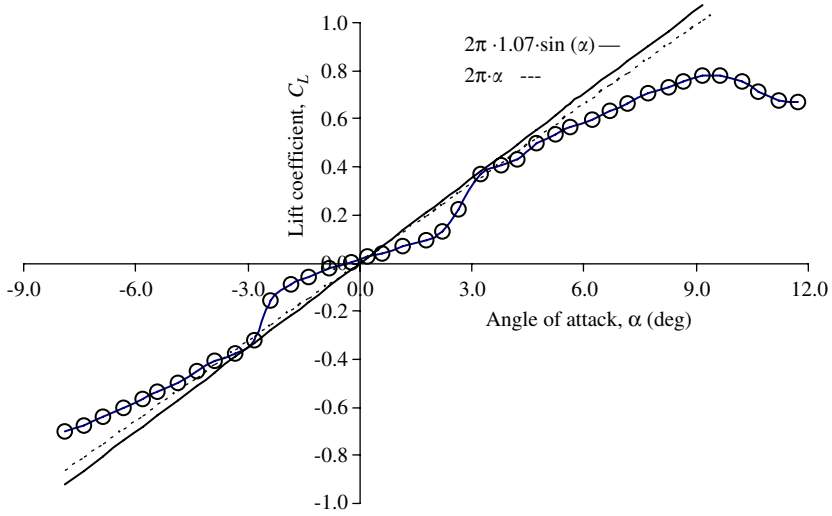

Fig. 1. Experimental, and inviscid, C_L versus α curve for a 2D NACA0009; $Re_c = 5 \times 10^4$, $Tu < 0.08\%$. Adapted experimental data from Fig. 16 of Lutz et al. (2001).

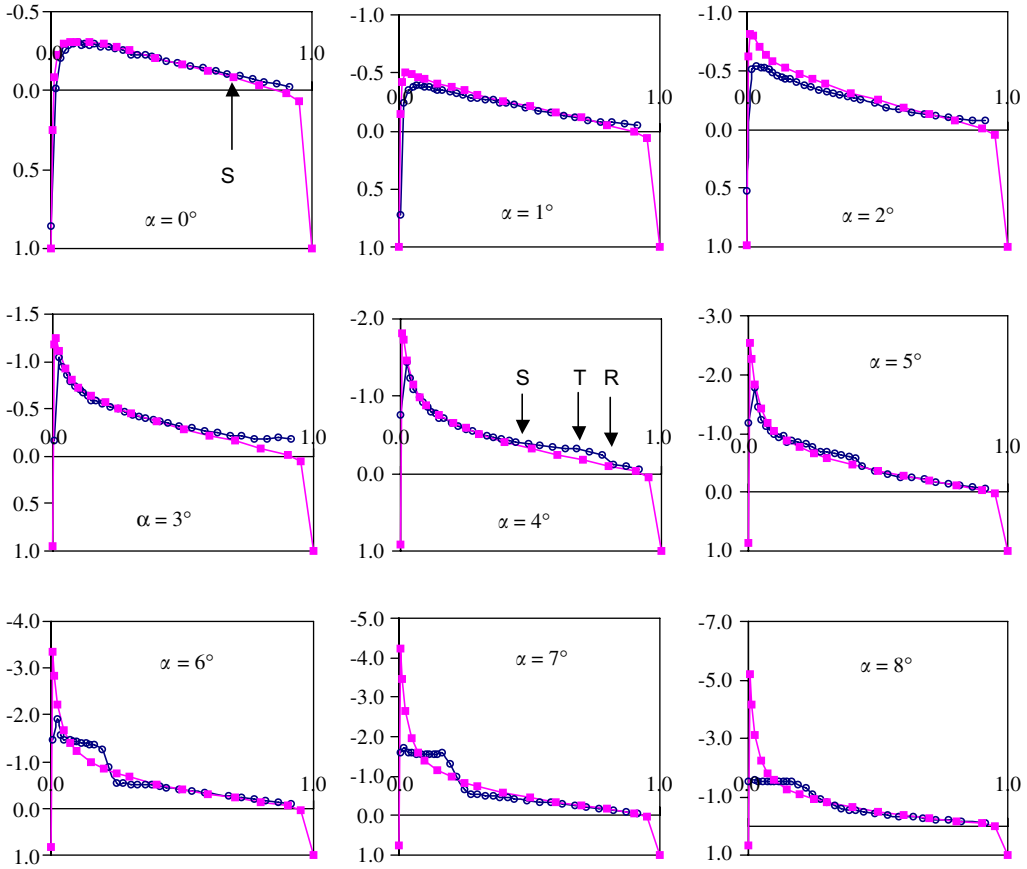

Fig. 2. Experimental (○), and inviscid (■), C_p versus x/c distributions on the suction side; 2-D NACA0009, $Re_c = 5 \times 10^4$, Tu < 0.08%. Adapted experimental data from Fig. 13 of Lutz et al. (2001).

observed by Huang and Lee (1999) on the NACA0012 discussed earlier. In addition, they showed that an increase in the free-stream turbulence level had for effect to significantly shorten the bubble length. The effect was most important for Tu < 0.45%. Above this value, no further significant changes were observed. Jacobs and Sherman (1937) as well noted that the NACA0012 exhibited laminar trailing edge separation for low angles of attack and low Reynolds numbers.

1.3. Wake characteristics

Transitional flow is not restricted to the boundary layer or the free-shear layer in the close vicinity of the airfoil surface. Flow regime transitions can occur in the wake of an airfoil. More specifically, flow oscillations presenting similar characteristics to the bluff-body von Kármán type vortex shedding have been observed in the wake of a wing in static conditions (Huang and Lin, 1995; Lee and Huang, 1998; Huang and Lee, 2000; William-Stuber and Gharib, 1990). Strouhal numbers ranging from 0.55 at small angles of attack to 1.1 at 90° were calculated for a NACA0012 wing. Furthermore, for angles of attack near stall, and below, a dependency of the Strouhal number with the Reynolds number has also been noted; lower Re_c numbers lead to lower St numbers (Huang and Lin, 1995). Four different modes of vortex shedding are defined. They are classified as laminar, subcritical, transitional and supercritical. The type of mode present depends on Reynolds number, angle of attack and turbulence intensity (Lee and Huang, 1998; Huang and Lee, 2000). For low Reynolds number, any vortex shedding regime can exist depending on angle of attack. Small angles are characterized by the laminar mode where the vortex shedding has a well-defined frequency. As the angle of attack is increased through the subcritical and then the transitional states, the wake periodicity disappears and reappears again, but superimposed by turbulent fluctuations in the supercritical mode. For high Reynolds numbers, the laminar and transitional modes are not present.

1.4. Aeroelastic oscillations

The richness and complexity of transitional Reynolds numbers aerodynamics phenomena observed for the static case act as a preamble to the appreciation of the aeroelastic problem. From the aeroelastic point of view, the aerodynamics can be treated as either an external force that acts on the airfoil, or as a system component that is coupled to the airfoil motion in a feedback relationship. Stall flutter is an example of the latter. This specific problem is complex but it is not strictly a low or high Reynolds number issue. It is a high angle of attack problem, as is the related dynamic stall phenomenon, which has been investigated at length but has yet to be fully solved. Stall flutter can occur either in bending or in torsion, although the physical mechanism is slightly different in each case. The bending motion becomes unstable simply as a result of the negative lift curve slope associated with static stall. The torsional motion instability requires dynamic stall to have occurred; hence, accurate modelling of both unsteady aerodynamics and separated flow is needed. The growing oscillatory motion then settles on a self-sustained or limit cycle oscillation (LCO).

For strictly low-to-moderate Reynolds numbers, self-sustained aeroelastic oscillations have also been reported but to a much lesser extent in terms of depth and scope of investigation. This is exemplified by the very small number of publications that are spread over the last 60 years. In 1947, Lambourne (1947) briefly reports, as part of a larger experimental study on classical flutter, pitching oscillations of the flutter model used in the experiment. They occur at approximately the natural frequency of the model. He calls the phenomenon "low wind speed oscillations". Surprisingly, neither the Reynolds number, nor the turbulence intensity for that matter, is given. Our calculations, based on an approximate guess of the model chord indicate the following range for the appearance of the oscillations: $4.0\times10^4\leqslant \mathrm{Re}_c\leqslant 7.5\times10^4$. Lambourne associates the oscillations with transition of the airflow occurring at some critical Reynolds number and attributes them to the presence of negative aerodynamic pitching damping. Seemingly similar oscillations are reported in 1951 by van de Vooren and Bergh (1951). While the range of Reynolds numbers for which they appear is again not given, our calculations indicate the following: $8.2\times10^4\leqslant \mathrm{Re}_c\leqslant 2.7\times10^5$. These "spontaneous oscillations", as they are labelled by Lambourne, occur at discrete values corresponding to the, mainly torsional, natural frequencies of the elastic wing, and are of small amplitude. The addition of a trip wire at $0.1c$ suppresses the oscillations completely. The phenomenon is explained on the basis of the classical stability theory of the laminar boundary layer.

Mabey et al. (1987) report violent LCOs of a symmetric half model at zero angle of attack and at Reynolds numbers one order of magnitude higher ($\mathrm{Re}_c\sim6\times10^6$) than in the previous observations. These oscillations occur in the wing's first bending mode of the flutter model at about 10 Hz when the transition is free; whereas fixing transition at 5% of the chord by boundary layer tripping suppresses the oscillations. An explanation is provided by applying quasi-steady aerodynamics, and the concept of an effective angle of attack ($\dot{y}/U$) arising from the bending motion, to describe the effect of the boundary layer transition and its movement on aerodynamic damping. The explanation is critiqued by Ericsson (1988), who later clarifies his point via the concept of the moving wall effect (Ericsson, 1990). He also highlights the difference in the flow mechanism between bending and pitching motion. In the former case, aerodynamic damping is provided by the bending motion itself, via $\dot{y}/U$, whereas for pitching motion it is the time lag (unsteady effects) that affects the damping.

The reporting of these oscillations was for the most part anecdotal and cursory. This paper aims at providing a much more focused treatment of aeroelastic self-sustained oscillations, where low Re effects are believed to play a fundamental role. To the authors' knowledge this is the first time that aeroelastic LCOs associated with low Re effects have been systematically studied and reported in the public literature. Although the problem is similar to stall flutter in so far as separated flow is involved, it occurs at very low angles of attack and for a limited range of Re numbers. This is a significant finding. Accordingly, this work focuses on the low-to-moderate range of Reynolds numbers by presenting and discussing an experimental investigation of periodic self-sustained pitch oscillations of an aeroelastic airfoil observed for $4.5\times10^4\leqslant \mathrm{Re}_c\leqslant 1.3\times10^5$. The experimental apparatus is first described along with the wind tunnel facility. Results consisting of the aeroelastic dynamics and wake velocity measurements are then given and discussed.

2. Experimental set-up

2.1. Aeroelastic apparatus

The apparatus is a two-degree-of-freedom system, composed of a rigid wing moving in translation (plunge, h) and in rotation (pitch, θ), as shown in Fig. 3. The apparatus is capable of exhibiting fundamental wing aeroelastic phenomena, both linear and nonlinear, such as flutter, LCO and response to external turbulence. Although an original design, it has

been inspired by similar apparatus at the Institute for Aerospace Research of the National Research Council of Canada, described in Marsden and Price (2005), and at Texas A&M University (O'Neil et al., 1996).

The wing profile is the standard NACA0012. As alluded to in the Introduction, its aerodynamic characteristics are relatively well known. An abundance of published data exists for this profile in steady conditions, namely in terms of angle of attack, (high) Reynolds number and aspect ratio. Some of its aerodynamic properties in unsteady conditions and separated flow have also been studied at length. However, low Reynolds number effects, vortex shedding and the influence of external turbulence are domains that remain to be fully explored.

The wing span is $s = 0.61$ m and its chord is $c = 0.156$ m, thus, giving an aspect ratio of AR = 3.9. The wing is made of an external aluminium frame surrounding a foam core and covered by fibreglass-epoxy. A 0.015 m diameter fibreglass rod is connected at each end of the wing via an attachment which mates to a series of screw holes staggered chordwise along the ends of the wing, thus enabling the axis of rotation (elastic axis, EA) of the wing to be changed. The wing is installed vertically in the test section of the wind tunnel to isolate its motion from the effect of gravity. As shown in Fig. 3, the support structure located outside the tunnel comprises two similar top and bottom translating sub-systems. Each of these sub-systems has a circular pulley that converts wing rotational motion into translation spring elongation. The equivalent torsional stiffness coefficient for the complete rotation mechanism is given by K_s. Plunge motion of the wing occurs via the translation of the two rectangular plates (translating sub-systems). Plunge stiffness is provided by two translation springs connected to each plate on one end and to a support structure fixed to the tunnel wall at the other end. One of the springs on each plate acts via a circular pulley. The top and bottom pulleys are connected through a vertical rod thus constraining the top and bottom plates to move as one unit. Further details are provided by Poirel et al. (2003). Both the pitch and plunge dynamics are measured with rotary potentiometers and are recorded via a National Instruments PCI-6034E A/D card using a LabVIEW based data acquisition system in which the sampling rate is set at a nominal value of 1 kHz. For the range of oscillation amplitudes tested, $\theta_{max} < 5.5^\circ$, the potentiometer design specifications allow oscillation frequencies to be measured up to 330 Hz. The raw data can then be processed through a Butterworth filter programmed in LabVIEW.

In this work, the motion is restricted to pitch alone, with plunge motion held fixed; this is equivalent to having an infinite stiffness in plunge. Table 1 provides a summary of the physical and geometric properties of the apparatus in its nominal configuration, as relevant to this work. These have been obtained by direct measurement, except for the structural stiffness coefficient which has been calculated from measurements of the translation spring coefficient and circular pulley radius, and except for the structural inertia and damping coefficient which have been calculated from free response test in still air.

The basic assumptions in defining the pitch stiffness and damping coefficients, K_s and D_s, respectively, are that the system can be represented as a linear single degree-of-freedom and that viscous damping is an appropriate model to account for the structural nonconservative forces. The linear viscous damping model is questionable from the point of view of the physical dissipative mechanisms, which are mainly dry friction in the ball bearings and spring compression. However, from a phenomenological point of view, the model is relevant as demonstrated in Fig. 4, which shows the free response of the wing in still air.

The system state is initially at its equilibrium point, $\theta = 0^\circ$, until an initial displacement is given at $t \approx 4.5$ s. The decaying and oscillating free response is typical of a linear single-degree-of-freedom mass-spring-dashpot system.

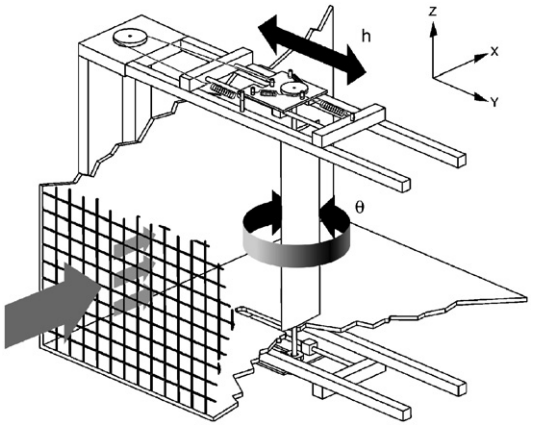

Fig. 3. Schematic of the aeroelastic apparatus.

Table 1
Aeroelastic apparatus nominal physical and geometric properties

x_θ	0.15	Unitless
a_h	−0.63	Unitless
I_s	0.00135	kg m^2
m_θ	0.771	kg
K_s	0.30	N m/rad
D_s	0.002	N m s
c	0.156	m
S	0.61	m

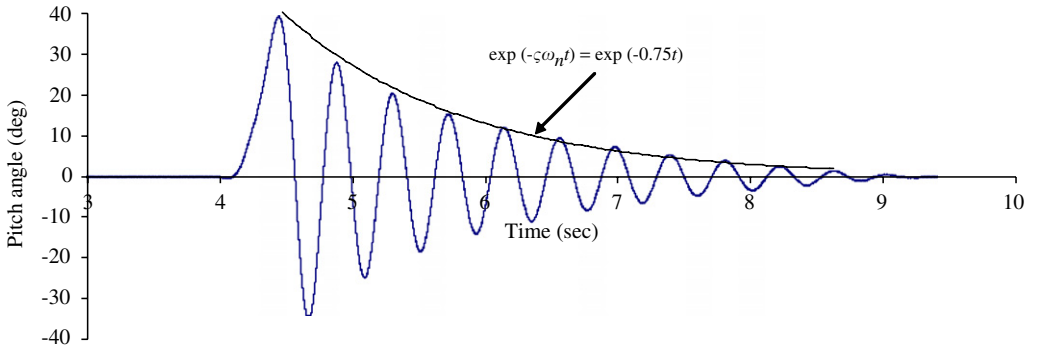

Fig. 4. Free response in still air (initial condition given at $t \approx 4.5$ s).

Superimposed on the time response is an exponential function which has for coefficient the mean of the real part of the eigenvalue, $\beta = -\zeta\omega_n$, calculated at every cycle. Although not perfect, the fit is very good. The damping ratio is calculated using the logarithmic decrement. Its mean value is $\zeta = 0.05$. The mean damped natural frequency is $\omega_d = 15.0$ rad/s, or 2.4 Hz.

We have also investigated the variation in frequency and damping between each cycle and between different free response tests performed at different days. The overall variations are expressed in terms of the coefficient of variation (COV = standard deviation/mean): COV$\beta = 35\%$ and COV$\omega = 2\%$. These values are representative of real life structures such as aircraft wings (Poirel et al., 2005). In general, the variations, or uncertainties, originate from three sources. They are measurement or observational noise, dynamical noise and basic modelling assumptions such as linearity. In our case, the former type is probably not as important since the (structural) system is simple and low-dimensional, and the response can be measured with relative ease and then treated with proper filtering. On the other hand, dynamical noise, which expresses the sensitivity of the system to its environment, and the inherent linearity assumption of viscous damping are likely to be more relevant contributions. In this regard the structural stiffness, represented by the natural frequency, is insensitive to environmental factors and appears to be free of any nonlinear contamination. No significant differences have been noted between test days and conditions, and between cycles. The greater variations observed in the damping are caused by an enhanced sensitivity to test conditions and by the assumption of linear viscous damping. For example, in addition to cycle-to-cycle random variations, we have observed a slight but noticeable increase in damping as the oscillation amplitude dampens during any particular free response test in still air.

2.2. Wind tunnel facility

The experiments are performed in the RMC wind tunnel, illustrated in Fig. 5. It is a closed circuit low speed tunnel powered by a 75 kW three-phase motor. The flow velocity ranges from 4 to 60 m/s, and is controlled by varying the fan speed. These velocities result in possible Re_c between 40 000 and 630 000. The test section measures 0.76 m × 1.08 m. End-plates are installed close to the wing tips to minimise 3-D effects. The gap between the wing tips and end plates is 7 mm, which is equivalent to 1% of the span. The solid blockage ratio, including the wing, rods and plates, is 5%.

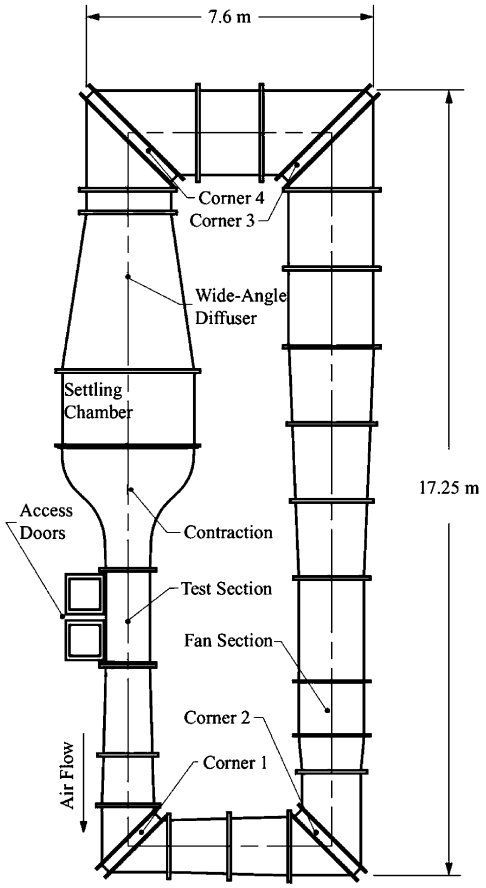

Fig. 5. The low-speed wind tunnel.

The free-stream velocity is measured with a pitot-static tube located at the entrance of the test-section and linked to a manometer. The flow temperature is also recorded with a thermocouple placed at the exit of the test-section. Unsteady flow measurements are obtained with a hot-wire anemometer and an X-wire probe. The probe is mounted to measure the longitudinal (x) and normal (y) components of the velocity, u and v, respectively. Data acquisition is conducted using DISA-56C17 CTA bridges and DISA-56N20 signal conditioning units. The data are sent through a high-pass filter set at 1 Hz and a low pass filter at 10 kHz. For the range of airspeeds considered in this work, a maximum turbulence intensity level ($\mathrm{Tu} = u'_{\mathrm{rms}}/U$) of no more than 0.15% exists (using the more complete definition of turbulence intensity, $\mathrm{Tu} = \sqrt{\frac{1}{2}(u'^2_{\mathrm{rms}} + v'^2_{\mathrm{rms}})}/U$, it is 0.2%).

3. Experimental results

3.1. Airfoil dynamics

The results presented are for the apparatus with its nominal properties listed in Table 1, and for various pitch stiffness coefficients, K_s, and location of the elastic axis, a_h. The springs, which are always in tension, were adjusted to set the equilibrium point at $\theta = 0^\circ$; the plunge is fixed at the centre of the test-section. Particular care was taken for the precise zeroing of the no-flow equilibrium point, as the aeroelastic response is sensitive to its location. The experiments were conducted in such a fashion as to track the self-sustaining oscillations of interest since, for certain pockets of airspeed, we noted a sensitivity to initial conditions and the appearance of co-existing attractors; hence, initial conditions were chosen accordingly. The data were recorded for at least 40 cycles of oscillations in order to ensure that steady state was

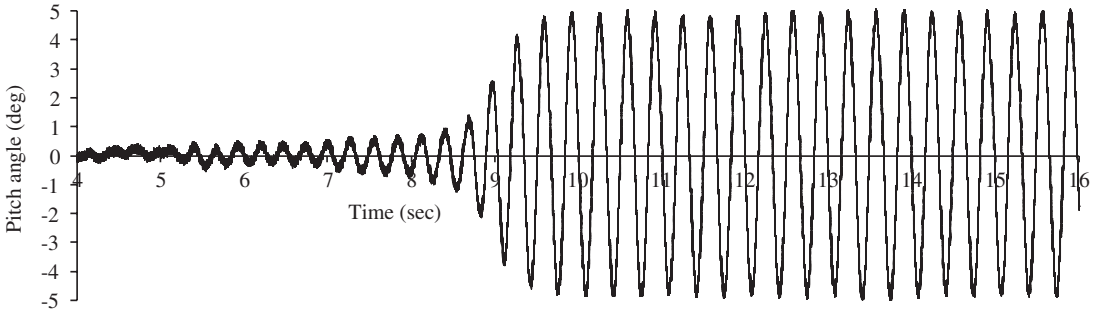

Fig. 6. Typical time response. Nominal configuration, $U = 7.5\,\mathrm{m/s}$.

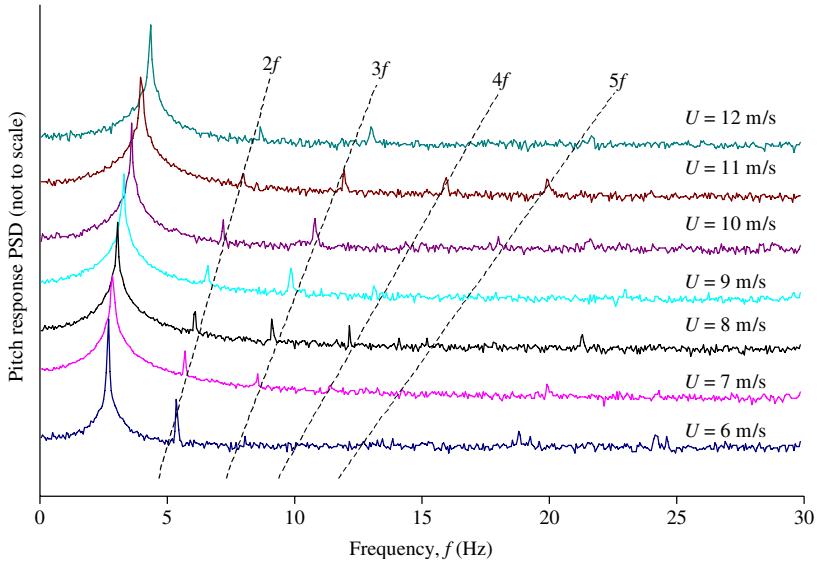

Fig. 7. Pitch response frequency spectrum for different airspeeds; nominal configuration. The curves are staggered by a factor of 100.

achieved. Two different sampling rates, 1 and 5 kHz, were used, depending on the data reduction requirements. Several runs, at different days and hours, were made at each test point in order to evaluate repeatability of the observed dynamics. The temperature was also monitored in an effort to evaluate its potential effect on the response. A baseline temperature of 21°, with variations between 19° and 24°, were recorded.

The behaviour is exemplified in Fig. 6. The time response shows the loss of stability of the equilibrium point after a small external perturbation is given to the system, followed by re-stabilization on an oscillatory state. The oscillations exhibit essentially simple harmonic motion. They naturally appear for airspeeds between approximately $U = 5$ and $12\,\mathrm{m/s}$ ($4.5 \times 10^4 \leqslant \mathrm{Re}_c \leqslant 1.3 \times 10^5$). Outside of this range the oscillations are not sustained.

There is a dominant frequency as shown in Fig. 7, which gives the spectral content of the steady state oscillations for a range of airspeeds. In addition to the main peak at the fundamental frequency, f, weaker even and odd superharmonics are displayed. Note that the relative intensity of the second harmonic to the third harmonic decreases with airspeed. No distinct features are noticed at higher frequencies. The PSDs were obtained from the average of 24 FFTs, each calculated using 16 384 time steps, for a total of 393 216 time steps. The input pitch data was recorded at every 0.001 s (sampling rate of 1000 Hz), resulting in a frequency resolution $\Delta f = 1/(N\Delta t) = 0.061\,\mathrm{Hz}$.

3.1.1. *Effect of structural stiffness*

Fig. 8 presents the amplitude and fundamental frequency of the oscillations for three different values of the pitch stiffness coefficient. The nominal configuration, where both the bottom and top pitch springs of the apparatus are enabled, results in $K_s = 0.30\,\mathrm{N\,m/rad}$; disabling the top spring and then both springs result in $K_s = 0.15$ and

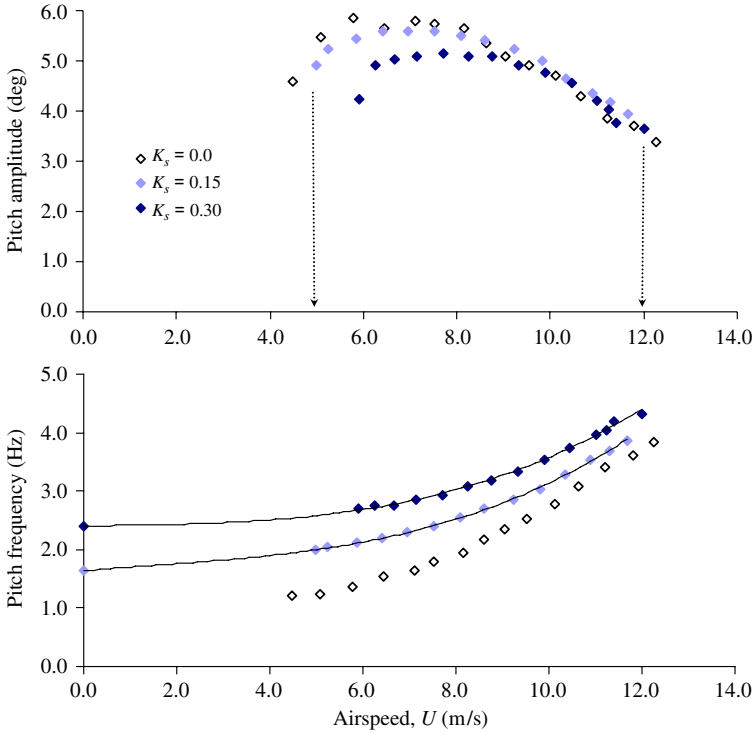

Fig. 8. Amplitude and frequency of oscillation for various stiffness coefficients. Nominal position of the elastic axis (position A).

0.0 N m/rad, respectively. In this last case, there is no structural stiffness. The oscillations are observed in all three cases. The error in the airspeed is ± 0.2 m/s and is mainly due to the resolution of the manometer from which the free-stream dynamic pressure is read. The error in the pitch amplitude is more difficult to assess due to the sensitivity of the response. For the higher airspeeds (over 8 m/s), it is about $\pm 0.2^\circ$ and is mainly due to cycle-to-cycle noisy amplitude fluctuations in the time response, and the position of the no-flow equilibrium point. For the lower airspeeds (under 8 m/s), the error is assessed at a higher value of about $\pm 0.3^\circ$. In this region, the response amplitude is more sensitive to experimental conditions and varies from test to test within this error margin. On the other hand, the frequency is much less sensitive to experimental conditions at any of the airspeeds tested.

In general, the configuration with zero structural stiffness is conducive to a larger range of airspeeds for which the oscillations are observed. The probable cause is that the friction that would be induced by the spring motion is not present in this case. In addition, both plots show that the responses of the three stiffness cases tend towards the same values with increasing airspeed. For the amplitude, there is a collapse of the responses for airspeeds above 8 m/s. For the frequency, the convergence of the three curves can be explained by the following. At low airspeeds, the oscillation frequency is mainly governed by the structural stiffness, which is significantly different for the three cases, whereas at larger airspeeds, the aerodynamic stiffness, being a function of airspeed, becomes dominant. Note that the structural natural frequencies are also shown on Fig. 8, and are clearly aligned with the extrapolation of the oscillation frequency curves towards the zero airspeed point.

3.1.2. *Effect of the elastic axis (EA) position*

Two other positions of the elastic axis were investigated, one ahead (B) and one aft (C) of the nominal position (A). Their locations are shown in Fig. 9. Note that they are equidistant. Also note that positions A ($0.18c$) and B ($0.10c$) are ahead of the $\frac{1}{4}$ chord point ($0.25c$) whereas position C is located slightly behind at $0.27c$.

Their effect is shown in Figs. 10 and 11. This is for the wing in its nominal configuration as per Table 1, except of course for a_h which varies. The same general trends are observed for all positions of the elastic axis, including the previous case (EA at A), with one notable exception. For the EA at location C (Fig. 11), no results are shown for the zero spring (no structural stiffness) since the pitch motion was erratic and had a large amplitude. Considering that this position is behind the $\frac{1}{4}$ chord point, it is suspected that the wing is in divergence conditions. We also note a clear change

in trends in the frequency plot for the EA at C between airspeeds below and above 8 m/s. A more detailed analysis is provided in Section 4.

3.1.3. *Sensitivity to initial conditions and flow perturbations*

Other steady state dynamics, or attractors, co-exist for the same conditions, namely an equilibrium point and other oscillation types. However, they are generally not as stable as the dynamics presented here. For instance, if the wing is initially set at zero initial conditions it will generally remain in this equilibrium position for all airspeeds tested, unless the flow, or airfoil, is given some perturbations. This is exemplified in Fig. 6 where the wing departs from its initial state at the equilibrium point toward an oscillatory state after the wind tunnel door has been slightly opened and then closed back. Generally speaking, the oscillations reported in this paper will appear for any nonzero initial conditions.

The aeroelastic oscillations are not very sensitive to isolated flow perturbations. As long as the flow is initially perturbed or the wing is given an initial condition they will appear. However, they are sensitive to continuous flow perturbations such as due to the presence of objects placed upstream. Blunt objects placed in the vicinity of the wing tend to either suppress the oscillations or make them intermittent. On the other hand, the addition of aerodynamic

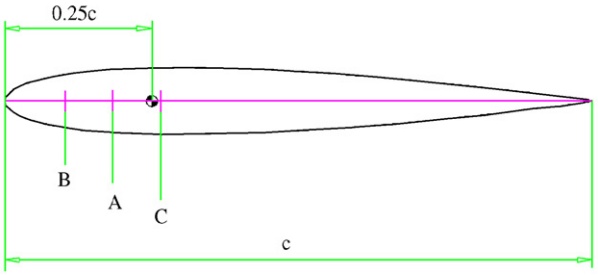

Fig. 9. Position of the elastic axis (EA).

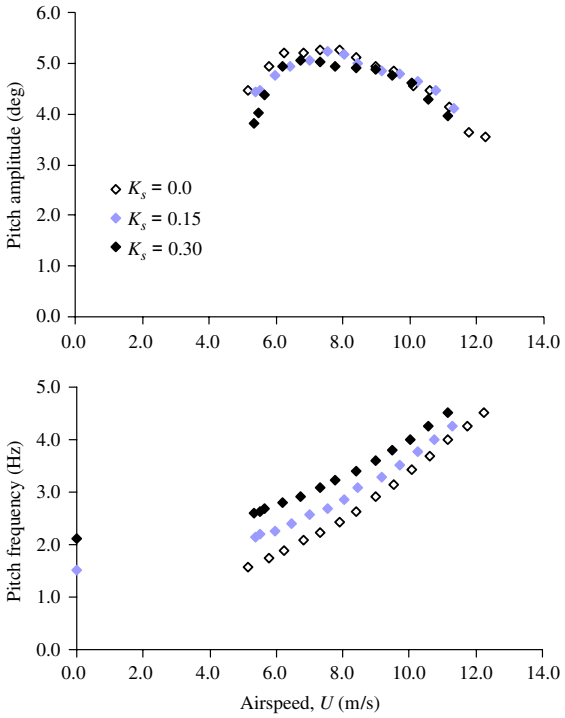

Fig. 10. Amplitude and frequency of oscillation for various stiffness coefficients. EA at B.

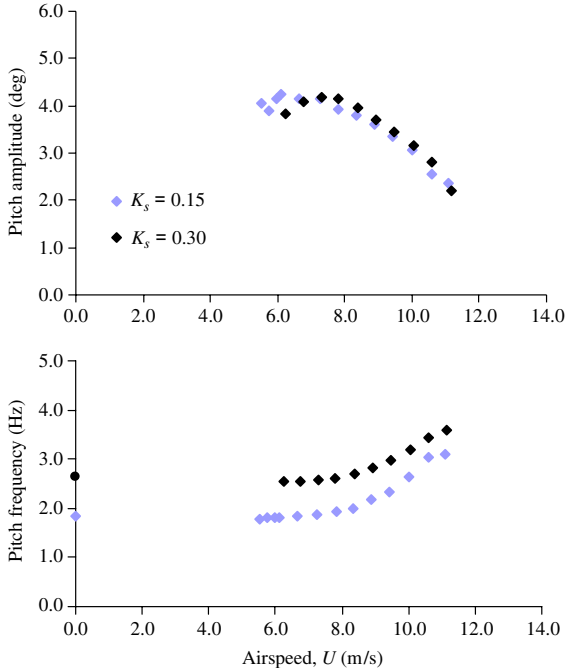

Fig. 11. Amplitude and frequency of oscillation for various stiffness coefficients. EA at C.

fairings around the connecting rods (between the wing and moving supporting structure) and the removal of the end plates do not modify the behaviour or existence of the oscillations.

The presence of a turbulence-generating grid placed upstream was also investigated. For turbulence intensities greater than about 0.4% these oscillations disappear. Finally, the addition of adhesive sandpaper to the wing, running from the leading edge to the $\frac{1}{4}$ chord point, completely suppresses the self-sustained oscillations as well. In this case, if the wing is given some initial conditions, the pitch oscillations decay to zero in a similar fashion to the still air response shown in Fig. 4, expect with different frequencies and decay rates since the aeroelastic system parameters are a function of airspeed. The damped natural aeroelastic frequencies that we observed were very close to the expected values derived from a simple theoretical model based on unsteady thin-airfoil aerodynamics. Some additional details on the modelling are provided in Section 4.3.

3.2. Wake measurements

A hot-wire probe placed one chord length behind the airfoil in its wake provides additional information. Spectral information for the same wing configuration and airspeed as in Fig. 6 (nominal properties) is shown in Fig. 12.

The FFT parameters are the following: the number of data points $N = 32\,768$, sampling rate $= 5000$ Hz (i.e. $\Delta t = 0.0002$ s), $\Delta f = 1/(N\Delta t) = 0.153$ Hz, $f_{\mathrm{Nyq}} = 1/(2\Delta t) = 2500$ Hz, 16 averages (i.e. 524 288 time steps). The u' and v' spectra are shown in addition to the pitch spectrum. The peak at $f = 2.9$ Hz in the wake velocities corresponds to the pitch frequency of oscillation. Also present are superharmonics at $2f$ and $4f$ in the u' spectrum, and at $2f$ and $3f$ in the v' spectrum. Of further interest is the broad band peak at $f = 236$ Hz in the wake spectra. This high frequency peak is not observed in the pitch. However, we are cautious in affirming this observation since, although the potentiometer is rated up to 330 Hz, the fact that the baseline pitch spectrum increases for the high frequencies tends to indicate that its ability to measure oscillations over $\sim$200 Hz is to some extent suspect. Finally, the peak at 30 Hz observed in the pitch spectrum is attributed to electrical noise and has no impact on the wing dynamics.

When the wing is held completely fixed at $\alpha = 0^\circ$, the spectra clearly display a similar high frequency peak ($f = 253$ Hz) in both wake unsteady velocity components, as shown in Fig. 13, in addition to a multiple at $2f$. Furthermore, the peaks are sharp in both components. However, the most significant observation is the nonappearance of a peak in the vicinity of 3 Hz. As mentioned previously the peak at 30 Hz is of no consequence here. The FFT parameters are the same as for Fig. 12. Tests at fixed angles of attack of $\pm 3^\circ$ and $\pm 5^\circ$ were also performed. These

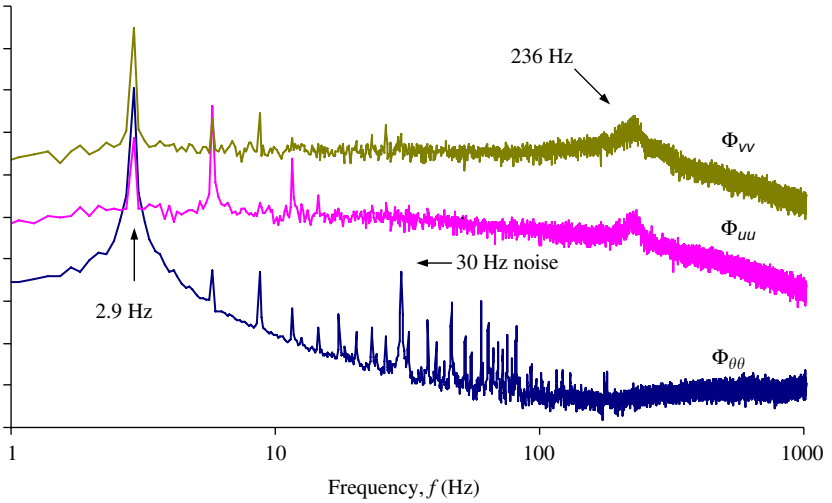

Fig. 12. PSD of u', v' and θ. Nominal configuration, $U = 7.5$ m/s. The curves are staggered by a factor of 100.

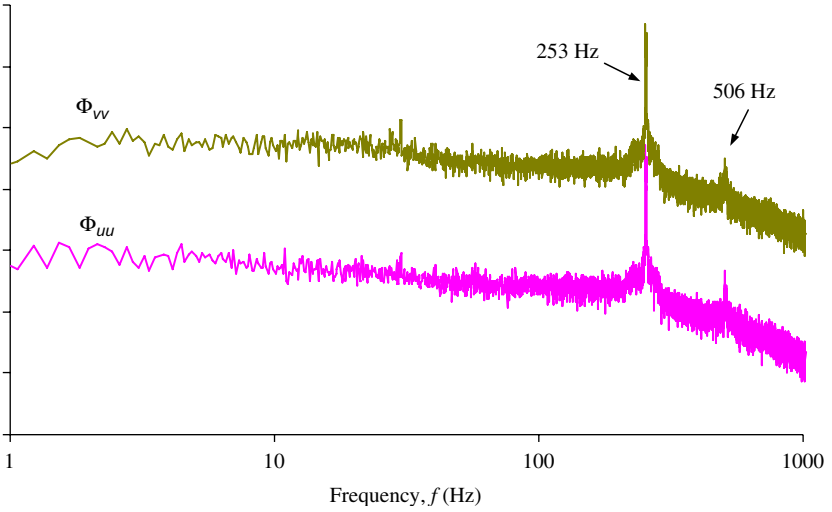

Fig. 13. PSD of u' and v'. Wing fixed at $\alpha = 0°$, $U = 7.5$ m/s. The curves are staggered by a factor of 100.

angles were chosen as they correspond to the range of oscillation amplitudes of the free wing. Not shown here, but the spectra of the u' and v' velocities at these angles also display a high-frequency peak. It is, however, not as sharp and is slightly displaced towards lower frequencies compared with the zero angle of attack case. Furthermore, no peak is observed at 2.9 Hz or in its vicinity.

4. Discussion and theoretical perspectives

4.1. Forced versus self-sustained oscillations

In this section, it is argued that the aeroelastic oscillations are self-sustained, or limit cycle (LCO). Should the pitch motion be caused by the aerodynamics acting as an external force, we would expect to observe a periodicity in the flow corresponding to the pitch oscillations even if the wing is rigidly fixed. First, hot-wire measurements of the upstream flow (not presented here) do not show any periodicity in the upstream flow accounting for this behaviour. Similarly, the

wake velocities do not show any periodicity near the pitch oscillation frequencies for the case where the wing is held fixed. This is true for all angles of attack tested, as demonstrated in Fig. 13 for the zero angle of attack case. The spectra are nearly flat in the frequency range of interest ($1\,\text{Hz} < f < 4\,\text{Hz}$).

Expressing the 2.9 Hz pitch oscillation frequency as a Strouhal number gives an uncommonly small value of $\text{St}_T = 0.007$. However, as discussed earlier in Section 1.1, similar low frequencies ($\text{St}_T \leqslant 0.01$) in the flow have been reported for rigidly mounted airfoils at angles of attack near static stall (Jones, 1933; Broeren and Bragg, 2001, 1998; Zaman et al., 1989; Bragg et al., 1993, 1995). It was postulated that the flow oscillations were due to a periodic switching between stalled and unstalled states. According to Zaman et al. (1989) the flow oscillations are related to a transitional state of the boundary layer, and more specifically to a cyclic growth and bursting of the LSB, according to Broeren and Bragg (2001, 1998) and Bragg et al. (1993, 1995). Zaman et al. noted as well that the oscillation amplitude was large in the vicinity of the $\frac{1}{4}$ chord point and decreased steadily downstream. To investigate this potential cause for the pitch oscillations, we performed hot-wire measurements close to the airfoil surface at $c/4$ for a small (fixed) angle of attack. No periodicity of relevance was observed. This is not inconsistent with Broeren and Bragg (2001, 1998), Zaman et al. (1989) and Bragg et al. (1993, 1995) since the reported flow oscillations were for high angles of attack; they did not observe any flow oscillations at low angles of attack.

The sharp peak displayed in Fig. 13 at 253 Hz expressed in terms of a Strouhal number based on the airfoil thickness gives $\text{St}_T = 0.62$. This value represents von Kármán vortex shedding, as demonstrated by Huang and Lin (1995), Lee and Huang (1998) and Huang and Lee (2000) for a static NACA0012 airfoil at this Reynolds number. In particular for these conditions ($\text{Re}_c = 7.8 \times 10^4$, $\alpha = 0^\circ$, $\text{Tu} = 0.2\%$), they showed experimentally that the wake is in the laminar vortex shedding mode. At this Reynolds number, increasing the angle of attack by only a few degrees transforms the shedding into the subcritical mode and then the transitional mode. Accordingly, the spectral peak broadens and shifts towards lower values with increasing angles of attack. This is what we have observed at $\alpha = 3^\circ$ and 5° for the fixed wing. It is also consistent with the broadening of the peak for the oscillating wing shown in Fig. 12 at $f = 236\,\text{Hz}$. This frequency is in effect an "average" of the instantaneous vortex shedding frequencies at each phase angle of the pitching motion; see Jung and Park (2005). Of further interest is the fact that, for all practical purposes, the pitch does not seem to respond to the von Kármán vortex shedding since no energy is observed in the pitch response PSD at $f \sim 250\,\text{Hz}$; see Fig. 12. However, as mentioned earlier, the potentiometer may not be fully operational at this high frequency.

These observations lead to the conclusion that the pitch oscillations for the free wing are not caused by vortex shedding, bubble bursting or, more generally, a pure periodicity in the flow, in the form of an external forcing. Instead, they are thought to be the consequence of a nonlinear coupling between the structure and the flow.

4.2. Aerodynamic stiffness, trailing edge separation and LSB

In any case, energy is transferred from the airflow to the structure to sustain the oscillations. Fig. 14 shows the aerodynamic moment coefficient, C_{Mea}, as a function of pitch angle throughout one cycle of oscillation. It is calculated from the two following dynamical equations where the right-hand side of Eq. (1) represents the structural forces. It should be realized that the aeroelastic rig acts in effect as a balance to measure the aerodynamic moment. The structural parameters are known (see Table 1), and θ is assumed to be a pure sinusoidal signal with a known frequency, and amplitude, as per Fig. 8. The S.H.M. assumption is justified since the superharmonics content in the pitch response is relatively small. It enables a more precise calculation of the $\ddot{\theta}$ and $\dot{\theta}$ terms compared with obtaining the time derivatives of θ via numerical differentiation of the noisy experimental time response. Thus,

$$M_{\text{EA}} = I_s\ddot{\theta} + D_s\dot{\theta} + K_s\theta \tag{1}$$

and

$$C_{\text{Mea}} = \frac{M_{\text{EA}}}{\frac{1}{2}\rho U^2 c^2 s}. \tag{2}$$

The fact that the ellipse is turning clockwise signifies that positive work is being done by the aerodynamic moment as the airfoil oscillates. The airflow produces negative aerodynamic damping and is consistent with positive energy being transferred from the airflow to the structure.

Also drawn is a line along the main axis of the ellipse, which can be interpreted as an equivalent linear static aerodynamic moment coefficient. The negative of the slope of this line, multiplied by $\frac{1}{2}\rho U^2 c^2 s$, is in turn interpreted as an equivalent linear aerodynamic stiffness coefficient K_a. The negative slope means that the aerodynamic stiffness is positive hence, is stabilizing. This makes sense since the elastic centre is ahead of the quarter-chord point for the

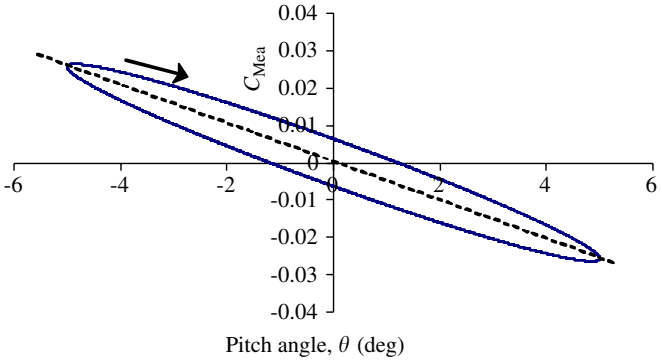

Fig. 14. Aerodynamic moment coefficient as a function of pitch angle. Nominal configuration, $U = 7.5\,\mathrm{m/s}$.

nominal configuration. The actual value of K_a calculated for the case shown in Fig. 14 is

$$K_a = -\frac{\mathrm{d}C_{\mathrm{Mea}}}{\mathrm{d}\theta}\tfrac{1}{2}\rho U^2 c^2 s = 0.15\,\mathrm{N\,m}. \tag{3}$$

The equivalent aerodynamic stiffness coefficient can also be estimated by assuming that the frequency of oscillation is the natural frequency of the aeroelastic system. This interpretation is consistent with the argument that the oscillations are self-sustained (Den Hartog, 1962), as opposed to forced in which case the oscillation frequency would correspond to the forcing frequency, unless there is lock-in. This immediately leads to the aerodynamic stiffness coefficient via the consideration of the structural stiffness coefficient and moment of inertia, as shown in Eqs. (4) and (5):

$$\omega = \sqrt{\frac{K_T}{I_s}} = \sqrt{\frac{K_s + K_a}{I_s}}, \tag{4}$$

$$K_a = \omega^2 I_s - K_s = (2\pi f)^2 I_s - K_s = 0.15\,\mathrm{N\,m}. \tag{5}$$

It must be emphasized that even though both Eqs. (3) and (5) provide the same estimate of an equivalent linear stiffness, this is an approximation since the aerodynamic stiffness is a nonlinear function of the pitch angle in this Re regime. Indeed, a close analysis of the pitch time response shown in Fig. 6 reveals that the frequency of oscillation of each cycle decreases with amplitude. At low amplitudes in the transitory regime, say at $t = 6\,\mathrm{s}$ where $\theta = 0.5^\circ$, the oscillation frequency is $f \approx 3.7\,\mathrm{Hz}$, whereas it is 2.9 Hz for the steady-state oscillations which occur at a higher amplitude. Associating the local oscillation frequency with a local aerodynamic stiffness implies that at low amplitudes the aerodynamic stiffness coefficient calculated from Eq. (5) is $K_a = 0.43$. In other words, in this range of angle of attack and Re number, the aerodynamics acts as a softening torsional spring.

This conclusion is corroborated by a comparison with experimental results from Huang et al. (1996) who observed similar trends on a rigid NACA0012 wing for the aerodynamic moment taken at the $\frac{1}{4}$ chord point. Note that the aerodynamic moment coefficients published by Huang et al. (1996) are one order of magnitude too large; this error was confirmed via email (in 2006). Comparing the Huang et al. corrected values of the aerodynamic moment coefficient at $\theta = 0.5^\circ$ and 5° for the same flow conditions in Re_c and Tu, their coefficients are $C_{mc/4} = -0.01$ and -0.028, respectively. For the problem investigated in this work, as shown on Fig. 14, $C_{\mathrm{Mea}} = -0.026$ at $\theta = 5^\circ$. Using a similar logic, making use of $K_a = 0.43$ and rearranging Eq. (3) to estimate C_{Mea} at $\theta = 0.5^\circ$, the aerodynamic moment coefficient at this small angle is $C_{\mathrm{Mea}} = -0.006$. Perfect agreement with Huang et al. is not expected due to the differences in the two problems, as for instance the exact position of the axis about which the moment is calculated; the EA is at 18% for the nominal case in this work. Nevertheless, the values of the two sets of coefficient are close to each other and the trend is the same, thus adding to the validation process of both the analysis and subsequent conclusions.

The large aerodynamic stiffness coefficient that exists at very low angles of attack ($K_a = 0.43$) makes physical sense since the airfoil likely experiences trailing edge laminar separation, as discussed in Section 1.2. Trailing edge separation induces a lower pressure on the suction side, which in turn, by virtue of the long moment arm between the separated zone and the elastic axis, forces the wing to pitch down. This moment is larger than when the flow is fully attached. For the case where a LSB exists at small but larger angles of attack, lower pressure is created within the LSB region also in comparison with the fully attached case; see Fig. 2. However, the LSB being closer to the elastic axis, the pitch down moment due to the low pressure is smaller than for trailing edge separation case, hence a smaller aerodynamic stiffness coefficient.

This physical interpretation leads to the speculation that, although the laminar trailing edge separation is stabilizing from a stiffness (static) point of view, as just discussed, it may be destabilizing from a damping (dynamic) point of view. The simple harmonic type oscillation that follows the loss of stability of the equilibrium point (Fig. 6) is consistent with a damping instability, and not with a stiffness instability. This would explain why there is a lower limit in Re number for the loss of stability of the equilibrium point and subsequent appearance of the oscillations. Under this limit there would be no trailing edge laminar separation; according to Huang and Lee (1999), trailing edge separation of a NACA0012 wing at 0° angle of attack, and 0.2% turbulence intensity, appears at $\mathrm{Re}_c = 5.4 \times 10^4$, which corresponds approximately to the lower limit where our aeroelastic oscillations appear.

On the other hand, it is speculated that the LSB is dynamically stabilizing, perhaps in the sense of the van der Pol model. Hence, as the oscillations grow from the equilibrium point a LSB appears and stabilizes the motion onto an LCO. These speculations are also consistent with our experimental results showing the disappearance of the oscillations for free-stream turbulence intensities larger than about 0.4%. Again according to Huang and Lee (1999), for $\mathrm{Tu} > 0.45\%$, transition and reattachment of the shear layer occur near the trailing edge even at zero angle of attack; hence at these turbulence levels there is no trailing edge laminar separation. However, it must be added that in light of Huang and Lee's results, our speculations fall short on one point, which is the explanation of the upper Re limit due to appearance of the LSB. They show that the LSB appears at 0° angle of attack, and 0.2% turbulence intensity, for $\mathrm{Re}_c > 9.1 \times 10^4$; our oscillations disappear at $\mathrm{Re}_c \approx 1.2 \times 10^5$.

4.3. Regimes of oscillations

As alluded to in Section 3.1, two broadly defined regions of different trends, below and above $U = 8\,\mathrm{m/s}$ ($\mathrm{Re}_c = 8.3 \times 10^4$), are noticed. For $U \leqslant 8\,\mathrm{m/s}$, not only is the pitch amplitude more sensitive to flow conditions, there is in general an inverse relationship between the pitch amplitude and the pitch stiffness coefficient as shown in Fig. 8 and to some extent in Fig. 10. A larger stiffness coefficient leads to a smaller oscillation amplitude. However, for $U \geqslant 8\,\mathrm{m/s}$, all amplitudes tend to collapse on one value regardless of the spring configuration; in corollary there is relatively little sensitivity to the flow conditions.

Any difference between the low ($U < 8\,\mathrm{m/s}$, $\mathrm{Re}_c < 8.3 \times 10^4$) and high ($U > 8\,\mathrm{m/s}$, $\mathrm{Re}_c > 8.3 \times 10^4$) airspeed regimes is less evident from the frequency graph of Fig. 8. The oscillation frequencies for the three stiffness cases tend to converge towards a common value with airspeed. This convergence was explained in Section 3.1.1 by the increasing importance of the aerodynamic stiffness, over the structural stiffness, as the airspeed is increased. However, plotting the oscillation frequencies in parallel with the aeroelastic natural frequencies provides more insight into the phenomenon and solidifies the interpretation of two distinct regimes. In doing so, however, is the problematic of defining the natural frequency. This is especially so considering the zero-spring case where the stiffness, hence the natural frequency, is solely due to the aerodynamics.

For the sake of discussion it is therefore assumed, here, that thin-airfoil aerodynamic theory provides a relevant model to obtain the natural frequency. Thin-airfoil theory assumes linear, inviscid and attached flow aerodynamics. Furthermore, unsteady aerodynamics effects are also modelled. In this regard, a two-state representation of Wagner's function is introduced; see Fung (1955). It physically represents the influence of the shed vorticity in the wake, due to the pitch motion, on the airfoil as it is convected downstream with speed U. A clarification is perhaps required with regards to the shed vortices. These vortices, or sheet of vorticity if the pitch motion is continuous, are not to be confused with the von Kármán vortices discussed previously. Although both types originate ultimately from viscosity, the cause to effect relationship between the vortices and pitch motion is fundamentally different in the two cases. The vortices, represented by Wagner's function, are an effect of pitch motion. On the other hand, the former type, known as the von Kármán vortex, can be the cause of the pitch motion if the airfoil is free to move. Another consideration for the modelling of unsteady aerodynamics is added mass. These terms physically represent the reaction force of the air displaced by the accelerated motion of the airfoil. Their importance is dictated by the airfoil/air mass ratio, μ. In this work, $\mu = 55$, which means that the wing is much more massive than the medium (air) in which it oscillates. Added mass terms are therefore not very significant; they are, nevertheless, retained. Wagner's two-state representation introduces two additional states which couple with the structural forces to make the aeroelastic model a coupled two-degree-of-freedom problem. The details of the derivation are not essential here and can be found in Poirel and Price (2003). The system eigenvalues are then calculated. Two of them form a complex conjugate pair, from which the imaginary part is the aeroelastic system natural frequency. The aeroelastic natural frequencies, as derived from the linearized aerodynamic model, are shown in Fig. 15 for the zero-spring cases, along with the corresponding self-sustained pitch oscillation frequencies.

Note that, expressed in terms of a reduced frequency ($k = \omega b/U = 2\pi f b/U$), the natural frequencies are in the order of 0.1–0.2. Linear unsteady effects are generally considered to become important for $k > 0.05$, thus justifying to some

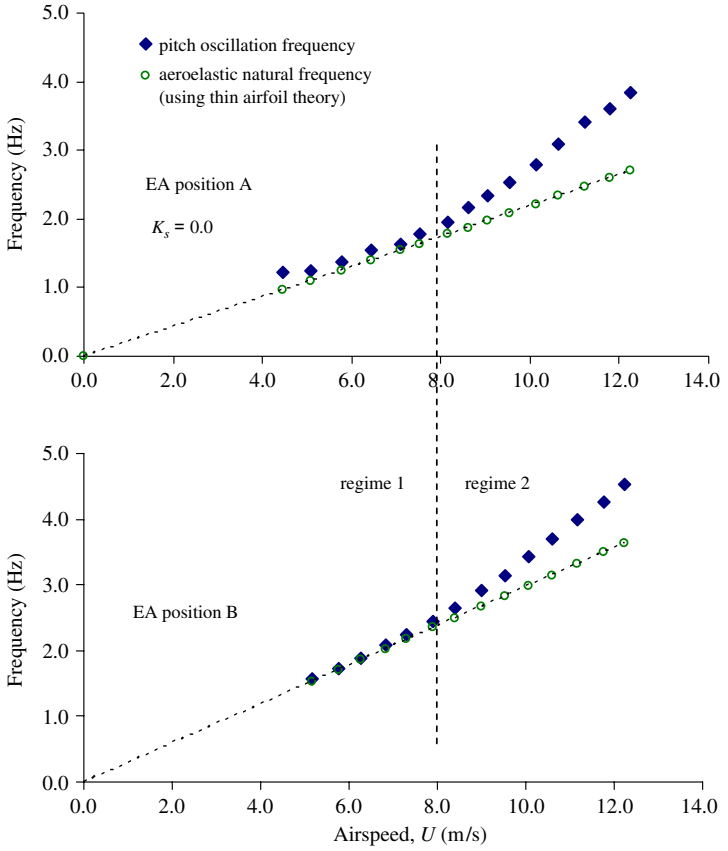

Fig. 15. Frequency of oscillations and aeroelastic natural frequency. EA at positions A and B; no springs.

extent the unsteady model. It is remarkable that although it is believed that the experimental self-sustained pitch oscillations originate from a nonlinear coupling between the structure and the low-to-moderate Re flow, their frequency is fairly close to the thin-airfoil theory model (which in many aspects represents high Re flow) for airspeeds below 8 m/s (i.e. $Re_c < 8.3 \times 10^4$). The fact that the oscillation frequencies are slightly larger than the model derived frequencies is consistent with the appearance of laminar trailing edge separation or a LSB since these phenomena induce a pitch down moment, hence increase the aerodynamic stiffness in comparison with the linearized model. For airspeeds above 8 m/s (i.e. $Re_c > 8.3 \times 10^4$), the split between the two curves clearly indicates another regime of oscillations.

Finally, additional evidence of the existence of two regimes, below and above $U = 8$ m/s, comes from Fig. 11 where the EA is at position C, and with one or two springs. The frequency plot also shows two regimes. For the region below 8 m/s, the oscillation frequencies are nearly independent of, or very slightly decreasing with, airspeed. In other words, the oscillation frequencies correspond to the pure structural natural frequency. This is indicative of a zero aerodynamic moment in this regime. From the point of view of linear aerodynamics it makes sense since the EA (position C) is located very close (slightly aft of the $c/4$ point), which is the (thin-airfoil) theoretical aerodynamic centre as well as the centre of pressure. Accordingly, it appears that in this regime the location of the centre of pressure is not affected by low Reynolds number effects, such as boundary layer thickness and possibly laminar trailing edge separation or the LSB. From a classical aeroelastic point of view, the wing is at the divergence boundary. On the other hand, for the other regime, above 8 m/s, the aerodynamic stiffness is not zero but positive, since the oscillation frequency increases with airspeed. This is another clear indication that there exist two different regimes for the self-sustained oscillations. A striking question emerges from this analysis, but for which we offer no answer at this time. It is to some extent paradoxical that the oscillations in regime 1 have characteristics that can be represented by inviscid thin-airfoil theory, which in effect models high Re aerodynamics; whereas the oscillations in regime 2 which occur at a higher Re than regime 1, do not. This perspective may offer some leads in understanding the physical mechanisms for the oscillations.

5. Conclusion

Considering the complexity of the flow around an airfoil in the 10^4–10^6 range of Reynolds numbers, as exemplified by the nonlinear C_L versus α relationship well below the stall angle, it is not surprising that the rigid but flexibly mounted NACA0012 airfoil exhibits a classical nonlinear dynamical behaviour in the form of a LCO. These oscillations are akin to stall flutter except that the latter is a high angle of attack problem, where flow separation occurs, and with minimal Re dependency. On the other hand, the oscillations reported in this work are of small amplitude and are centred about $\alpha = 0^\circ$. They also have a strong Re dependency. These attributes are significant departures from stall flutter. Their existence enlarges the domain of flow types susceptible of generating complex aeroelastic behaviour from the two traditional regimes, namely transonic and high angle of attack flows, to a third regime characterized by transitional Reynolds numbers.

It is hypothesized that the self-sustained oscillations originate from a nonlinear coupling between the free pitching airfoil and the low-to-moderate transitional Re flow, the fundamental supporting evidence being that no periodicity in the free-stream, nor anywhere in the flow field around and in the wake of the fixed airfoil, account for this behaviour. Furthermore, it is speculated that laminar trailing edge separation and the presence of a LSB play a crucial role. In particular, it is suggested that the oscillations are somehow initiated by laminar trailing edge separation when initial conditions are close to 0°, whereas the steady state limit cycle is associated with the presence of a LSB. Although no direct and explicit evidence of the presence of laminar separation and bubble have been provided, due to the nature of the experimental set-up which focused on the aeroelastic dynamics and wake characteristics, strong arguments supporting their existence do exist. First, the range of Reynolds numbers for which the oscillations are observed is consistent with the existence of these low-to-moderate Re aerodynamic phenomena. Second, published literature has demonstrated their presence on the NACA0012 wing, as well on similar shapes, for the same angles of attack, Reynolds numbers and free-stream turbulence intensity as investigated in this work. Third, boundary layer tripping mechanisms such as high free-stream turbulence intensity generated with a turbulence grid and surface roughness using sand paper have been shown to have a decisive impact on the existence, or destruction, of the pitch oscillations.

From a practical point of view, it is noteworthy to mention that the aeroelastic oscillations observed in this work may possibly exist in the form of flight dynamics oscillations (LCO of a rigid air vehicle). This is so since they appear regardless of the presence of structural springs.

Acknowledgements

The authors are thankful to Dr B.H.K. Lee of NRC/IAR for sharing ideas for the design of this apparatus. The support of the Department of National Defence, through the ARP program, and the Natural Sciences and Engineering Research Council of Canada (NSERC) are also gratefully acknowledged.

References

Abbott, I.H., von Doenhoff, A.E., 1959. Theory of Wing Sections. Dover Publications, Inc., New York.

Bragg, M.B., Heinrich, D.C., Khodadoust, A., 1993. Low-frequency flow oscillation over airfoils near stall. AIAA Journal 31 (7), 1341–1343.

Bragg, M.B., Heinrich, D.C., Balow, F.A., Zaman, K.B.M.Q., 1995. Flow oscillation over an airfoil near stall. AIAA Journal 34 (1), 199–201.

Broeren, A.P., Bragg, M.B., 1998. Flowfield measurements over an airfoil during natural low-frequency oscillations near stall. AIAA Journal 37 (1), 130–132.

Broeren, A.P., Bragg, M.B., 2001. Unsteady stalling characteristics of thin airfoils at low Reynolds number. In: Mueller, T.J. (Ed.), Fixed and Flapping Wing Aerodynamics for Micro Air Vehicle Applications, Progress in Astronautics and Aeronautics, vol. 195. AIAA, Reston, pp. 191–213.

Den Hartog, J.P., 1962. Mechanical Vibrations. McGraw-Hill Book Company, Inc., New York.

Dowell, E.H., Edwards, J., Stragnac, T., 2003. Nonlinear aeroelasticity. Journal of Aircraft 40 (5), 857–874.

Ericsson, L.E., 1988. Comment on aeroelastic oscillations caused by transitional boundary layers and their attenuation. Journal of Aircraft 25 (10), 975–976.

Ericsson, L.E., 1990. Effects of transition on wind tunnel simulation of vehicle dynamics. Progress in Aerospace Sciences 27, 121–144.

Fung, Y.C., 1955. An Introduction to the Theory of Aeroelasticity. Wiley, Inc., New York.

Gad-el-Hak, M., 1990. Control of low-speed airfoil aerodynamics. AIAA Journal 28 (9), 1537–1552.

Huang, R.-F., Lee, H.-W., 1999. Effects of freestream turbulence on wing-surface flow and aerodynamic performance. Journal of Aircraft 36 (6), 965–972.

Huang, R.-F., Lee, H.-W., 2000. Turbulence effect on frequency characteristics of unsteady motions in wake of wing. AIAA Journal 38 (1), 85–93.

Huang, R.-F., Lin, C., 1995. Vortex shedding and shear-layer instability of wing at low-Reynolds numbers. AIAA Journal 33 (8), 1398–1403.

Huang, R.-F., Shy, W.W., Lin, S.W., Hsiao, F.-B., 1996. Influence of surface flow on aerodynamic loads of a cantilever wing. AIAA Journal 34 (3), 527–532.

Jacobs, E.N., Sherman, A., 1937. Airfoil section characteristics as affected by variations of the Reynolds number. NACA Report 586.

Jones, B.M., 1933. An experimental study of the stalling of wings. Aeronautical Research Committee Reports and Memoranda 1588, His Majesty's Stationery Office, London.

Jung, Y.W., Park, S.O., 2005. Vortex-shedding characteristics in the wake of an oscillating airfoil at low Reynolds number. Journal of Fluids and Structures 20, 451–464.

Lambourne, N.C., 1947. An experimental investigation on the flutter characteristics of a model flying wing. British Aeronautical Research Council, Reports and Memoranda 2626.

Lee, H.-W., Huang, R.-F., 1998. Frequency selection of wake flow behind a NACA 0012 wing. Journal of Marine Science and Technology 6 (1), 29–37.

Lutz, T., Würz, W., Wagner, S., 2001. Numerical optimization and wind-tunnel testing of low Reynolds number airfoils. In: Mueller, T.J. (Ed.), Fixed and Flapping Wing Aerodynamics for Micro Air Vehicle Applications, Progress in Astronautics and Aeronautics, vol. 195. AIAA, Reston, pp. 169–190.

Mabey, D.G., Ashill, P.R., Welsh, B.L., 1987. Aeroelastic oscillations caused by transitional boundary layers and their attenuation. Journal of Aircraft 24 (7), 463–469.

Marsden, C.C., Price, S.J., 2005. The aeroelastic response of a wing section with a structural freeplay nonlinearity: an experimental investigation. Journal of Fluids and Structures 21, 257–276.

McCullough, G.B., Gault, D.E., 1951. Examples of three representative types of airfoil-section stall at low speed. NACA-TN-2502.

Mueller, T.J., 1985. Low Reynolds number vehicles. AGARD-AG-288.

O'Neil, T., Gilliatt, H., Strganac, T., 1996. Investigations of aeroelastic response for a system with continuous structural nonlinearities. In: Proceedings of the 37th AIAA SDM Conference, AIAA Paper 96-1390, Salt Lake City, USA.

Poirel, D., Price, S.J., 2003. Random binary (coalescence) flutter of a two-dimensional linear airfoil. Journal of Fluids and Structures 18 (1), 23–42.

Poirel, D., Clément, M., Bouchard, H., Vaivads, R., 2003. Qualification of an experimental aeroelastic apparatus at RMC. In: Proceedings of the CASI Ninth Aerodynamics Symposium, Montréal, Canada.

Poirel, D., Dunn, S., Porter, J., 2005. Flutter-margin method accounting for modal parameter uncertainties. Journal of Aircraft 42 (5), 1236–1243.

Tang, D.M., Dowell, E.H., 1992. Flutter and stall response of a helicopter blade with structural nonlinearity. Journal of Aircraft 29 (5), 953–960.

Tani, I., 1964. Low-speed flows involving bubble separation. Progress in Aeronautical Sciences 5, 70–103.

van de Vooren, A.I., Bergh, H., 1951. Spontaneous oscillations of an aerofoil due to instability of the laminar boundary layer. National Aeronautical Research Institute (NLR) F96.

White, F., 2006. Viscous Fluid Flow. McGraw-Hill, New York.

William-Stuber, K., Gharib, M., 1990. Transition from order to chaos in the wake of an airfoil. Journal of Fluid Mechanics 213, 29–57.

Zaman, K.B.M.Q., McKinzie, D., Rumsey, C., 1989. A natural low-frequency oscillation of the flow over an airfoil near stalling conditions. Journal of Fluid Mechanics 202, 403–442.